International Journal of Thermophysics, Vol. 15, No. 5, 1994

Thermodynamic Properties of Two Gaseous Halogenated Ethers from Speed-of-Sound Measurements: Difluoromethoxy-Difluoromethane and 2-Difluoromethoxy-1,1,1-Trifluoroethane

K. A. Gillis[1]

Received May 6, 1994

We present measurements of the speed of sound in gaseous difluoromethoxy-difluoromethane (CHF_2-O-CHF_2) and 2-difluoromethoxy-1,1,1-trifluoroethane (CF_3-CH_2-O-CHF_2). These measurements were performed in an all-metal apparatus between 255 and 384 K. We have obtained ideal-gas heat capacities and second acoustic virial coefficients from analysis of these measurements. Two methods of correlating the second acoustic virial coefficients, a square well model of the intermolecular interaction and a function due to Pitzer and Curl, are presented.

KEY WORDS: 2-difluoromethoxy-1,1,1-trifluoroethane; difluoromethoxy-difluoromethane; E134; E245; heat capacity; speed of sound.

1. INTRODUCTION

In response to the 1987 Montreal Protocol [1], the refrigeration industry is searching for suitable alternatives to the environmentally hazardous chlorofluorocarbons now widely used as refrigerants, foam blowing agents, solvents, etc. In many cases the thermodynamic properties of these proposed alternatives are unknown and cannot be calculated with sufficient accuracy to design efficient refrigeration systems. The National Institute of Standards and Technology (NIST) has an extensive program to gather the necessary data in order to satisfy the needs of the industry.

[1] Thermophysics Division, National Institute of Standards and Technology, Gaithersburg, Maryland 20899, U.S.A.

0195-928X/94/0900-0821$07.00/0

When the spectroscopic data available for a material are insufficient to calculate the ideal-gas heat capacity, flow calorimetry or sound-speed measurements are performed to obtain the desired information. It is well documented that precise and accurate speed-of-sound measurements are possible using acoustic resonators [2–11]. In recent years, this technique has been used to determine ideal-gas heat capacities of numerous compounds [12–16]. The temperature and pressure dependence of the sound speed $u(T, p)$ in gases can be represented by an acoustic virial expansion in the pressure p:

$$u^2 = (RT\gamma_0/M)[1 + (\beta_a/RT)\,p + (\gamma_a/RT)\,p^2 + \cdots] \tag{1}$$

Here the second and third acoustic virial coefficients are β_a and γ_a, respectively, R is the gas constant, M is the molar mass, and γ_0 is the ratio of the constant-pressure to the constant-volume ideal-gas heat capacity C_p^0/C_V^0. Fits of Eq. (1) to the speed-of-sound results yield values of $\gamma_0(T)$, $\beta_a(T)$, and $\gamma_a(T)$. The constant-pressure ideal-gas heat capacity is obtained from the relation

$$C_p^0/R = \gamma_0/[\gamma_0 - 1] \tag{2}$$

and is then fit by a polynomial to represent its temperature dependence. The virial coefficient $B(T)$ from the equation of state

$$pV_m/RT = 1 + (B/V_m) + (C/V_m^2) + \cdots \tag{3}$$

is related to $\beta_a(T)$ by the differential equation

$$\beta_a = 2B + 2(\gamma_0 - 1)\,T\frac{dB}{dT} + \frac{(\gamma_0 - 1)^2}{\gamma_0}\,T^2\frac{d^2B}{dT^2} \tag{4}$$

where V_m is the molar volume. The virial coefficients obtained from the solution to Eq. (4) generally have an imprecision comparable to, or lower than, that determined from conventional p–V_m–T measurements [7–16].

Our laboratory has previously used high-precision acoustic resonance techniques [12–14, 17] to deduce the ideal-gas heat capacities and acoustic virial coefficients for several proposed alternative refrigerants. For those measurements, the low-order acoustic resonances of a gas in a small spherical cavity were used to measure the sound speed $u(T, p)$ with a fractional uncertainty $\Delta u/u \approx 10^{-4}$. From the zero-pressure limit of the sound speed, the ideal-gas heat capacity C_p^0 was determined with a fractional uncertainty $\Delta C_p^0/C_p^0 \approx 1 \times 10^{-3}$. Using a model for the intermolecular potential in the analysis of the acoustic data, we obtained second virial coefficients $B(T)$

that were consistent with those determined from high-quality p–V_m–T measurements. The limiting factor in the measurement accuracy was the extent to which the gas composition could be characterized and maintained. Elastomers, used in vacuum seals and in the construction of transducers, within the sample environment caused sorption problems and, in one case, a change in the composition of the sample [17, 18].

Recently, we constructed and tested an all-metal cylindrical acoustic resonator with the objective of eliminating problems with elastomers mentioned above [18]. With this design, the sample was in contact with only stainless steel, gold, and nickel. An additional advantage of this design was that the transducers were outside the thermostatic fluid bath, thus extending the accessible temperature range for accurate acoustic measurements. The measurements presented in this paper were performed with this all-metal apparatus.

The present paper focuses on two fluorinated ethers: difluoromethoxydifluoromethane (E134) and 2-difluoromethoxy-1,1,1-trifluoroethane (E245).[2] We report[3] acoustic measurements of $u(T, p)$ in gaseous E134 for temperatures between 255 and 373 K and for pressures from 7 to 87 kPa. The ideal-gas heat capacity and the second acoustic virial coefficient, deduced from analysis of these data, are presented over the entire temperature range. The third acoustic virial coefficient is given for $T < 290$ K, where the data extend up to 75% of the vapor pressure. The acoustic measurements on E245 spanned the temperature range 277 to 384 K and the pressure range 10 to 50 kPa. Model square-well intermolecular potentials are provided for both gases for estimating the second density virial coefficient. At this time, no equation-of-state data exist for these gases with which we could compare our results.

2. APPARATUS, MATERIALS, AND PROCEDURES

The acoustic apparatus, shown schematically in Fig. 1, consisted of the resonator, two electroacoustic transducers, waveguides, and diaphragms. The temperature controlled fluid bath is shown to emphasize the spatial separation between the resonator and the transducers. The acoustic waveguides carried the sound between the resonator and the remote

[2] E134 and E245 are designations that were adopted by the American Society of Heating, Refrigerating, and Air-Conditioning Engineers. These designations for ether-based compounds, first proposed by W. L. Kopko, follow a numbering scheme that was originally adopted for ethane- and propane-based refrigerants, respectively [19].

[3] The results for E134 have been published elsewhere [17] as part of a manuscript devoted to the thermophysical properties of E134.

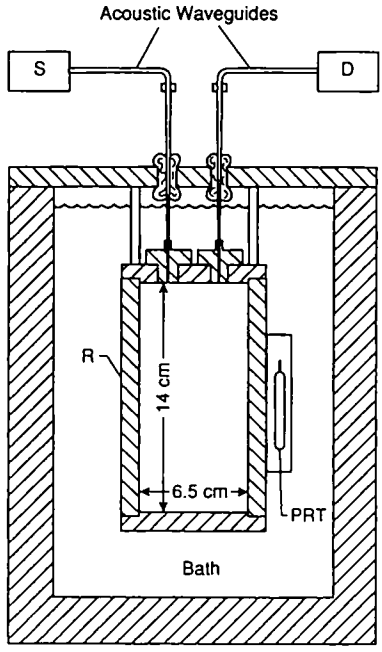

Fig. 1. Sketch of the apparatus, showing the resonator (**R**) in the temperature controlled environment, the remote source (**S**) and detector (**D**) transducers, and the waveguides.

transducers. The gas in the waveguides (argon or air) was separated from the test gas in the resonator by thin metal diaphragms whose vibration coupled the sound between the gases.

2.1. Resonator

For the measurements described in this paper, a stainless-steel cylindrical resonator, 14 cm long and 6.5 cm in inner diameter, was suspended vertically from the lid of the bath and into the thermostatic fluid. We chose a cylindrical resonator for these measurements because we needed lower resonance frequencies than could be achieved with a sphere of comparable volume. The frequency range was restricted to 1 to 8 kHz by the acoustic waveguides, which is discussed in the next section. The precision with which we can measure the sound speed in a cylindrical resonator is lower

than it is in a sphere because of viscous losses at the walls and the accompanying broader resonances. The accuracy of the measurement, however, continues to be limited by our knowledge of the gas composition.

The longitudinal portion of the cylindrical resonator was machined out of 304 stainless-steel tubular stock to a wall thickness of about 1.3 cm. Each end of the cavity was a type 304 stainless-steel flange, 1.3 cm thick, which fit into the cylinder with a clearance of less than 25 μm and was sealed with a gold O-ring. The inner surface of the cavity was polished to remove tool marks from machining.

2.2. Diaphragms and Waveguides

A schematic representation of a diaphragm assembly and an attached waveguide is shown in Fig. 2. The diaphragm was a stainless-steel disk 1 cm in diameter and 25 μm thick that had been electron beam welded around the circumference to a stainless-steel flange. Clearance was provided to allow the diaphragm to flex slightly in both directions under differential pressure. A chemically inert gold O-ring was used to form a vacuum-tight seal between the diaphragm assembly and the resonator. The diaphragm was flush with the inner surface of the resonator when the O-ring was fully compressed. The joint between the diaphragm assembly and the waveguide was sealed with Stycast 2850[4] epoxy for the initial measurements, but later it was brazed for use at higher temperatures.

Each waveguide consisted of a cylindrical tube leading from a transducer to a horn-shaped section. Each horn was made of thin-walled stainless steel and had an outside diameter that tapered exponentially from 0.33 cm at the junction with the extension tube down to 0.12 cm over a length of 15 cm. The horns were manufactured by Brüel and Kjær for use in probe microphones. An acoustic termination comprised of a specially designed metal screen was provided by the manufacturer in the small-diameter end of each horn, as shown in Fig. 2. The termination dampens resonances in the waveguides that would have occurred in its absence. The manufacturer's specifications for these horns show that the frequency response is flat between 30 and 8000 Hz, then drops 20 dB/octave above 10 kHz. The cylindrical extension tubes were stainless steel, with an outside

[4] In order to describe materials and experimental procedures adequately, it is occasionally necessary to identify commercial products by manufacturer's name or label. In no instance does such identification imply endorsement by the National Institute of Standards and Technology, nor does it imply that the particular product or equipment is necessarily the best available for the purpose.

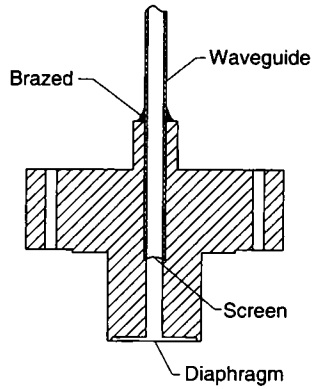

Fig. 2. Cross section through the diaphragm assembly, not to scale. The screen at the end of the waveguide is a resistive acoustic termination to dampen reflections.

diameter of 0.32 cm and 0.01-cm-thick walls, and were about 25 cm long. The gas in the waveguides was ambient air for the E134 measurements and argon for the E245. For the E245 measurements, the argon pressure was controlled to be 5 kPa above that of the test gas. Control of the pressure within the waveguides maximized the acoustic transmission through the diaphragms [18]. Thermal insulation was placed around the waveguides to attenuate fluctuations in the phase of the acoustic wave due to changes in room temperature.

2.3. Transducers

A stronger sound source was used in these measurements than in our previous apparatuses to overcome attenuation from two effects: (1) acoustic impedance mismatch between the gases and the diaphragms and (2) acoustic attenuation due to viscous damping through the screens. We found that a small (approximately 2-cm-diameter), commercially available earphone capable of dissipating a few watts was a satisfactory source. The source's small size made it easy to couple it to the small diameter waveguide. The detector was also small and sensitive over the frequency range of interest (1 to 10 kHz). It was made by Knowles Electronics, Inc., for use in hearing aids, and it had a rated sensitivity of

22×10^{-3} V/Pa at 1 kHz. To reduce the crosstalk between the transducers, they were sealed into airtight enclosures and isolated from their supporting structure.

2.4. Acoustic Modes of a Cylinder

For a cylindrical cavity with radius a and length l, the discrete values of the wavenumber k ($\equiv 2\pi/\lambda$) are known functions of a, l, and three nonnegative integers, K, N, and S [20]. The mode designated (K, N, S) has a wavenumber k_{KNS}. The symmetry of each mode is determined solely by (K, N, S): For example, (K, 0, 0) refers to purely longitudinal vibrations, (0, N, 0) describes azimuthal vibrations which circulate about the axis of the cylinder, and (0, 0, S) designates purely radial vibrations. The modes for which $N = 0$ are nondegenerate, and the modes with $N \neq 0$ are twofold degenerate. The unperturbed resonance frequency of mode (K, N, S) in a cylindrical cavity is given by

$$f^0_{KNS} = \frac{u}{2\pi}\left(\left(\frac{K\pi}{l}\right)^2 + \left(\frac{z(N, S)}{a}\right)^2\right)^{1/2} \tag{5}$$

where $z(N, S)$ is a root to $dJ_N(z)/dz = 0$ and $J_N(z)$ is the Nth order Bessel function. The actual resonance condition will occur at a slightly different frequency, $f_{KNS} = f^0_{KNS} + \Delta f_{KNS}$ because of the influence of several perturbations discussed in detail below. The half-width g_{KNS} of a resonance can be calculated if the energy loss mechanisms that are present in the cavity are known. Our analysis of the modes of the cylindrical resonator takes into account energy loss occurring in the bulk fluid and at the wall giving rise to the half-widths g^b_{KNS} and g^w_{KNS}, respectively. The half-width g^b_{KNS} is given by

$$g^b_{KNS} = \frac{\pi^2 f^3}{u^2}\left[\frac{4}{3}\delta_v^2 + (\gamma - 1)\,\delta_t^2 + \eta_b/\pi\rho f\right] \tag{6}$$

where η_b is the bulk viscosity, and γ is the ratio of the constant-pressure/constant-volume specific heats C_p/C_v at density ρ. The penetration depths δ_v and δ_t are defined below. The frequency f in Eq. (6) is just the resonance frequency f_{KNS}. The half-width g^w_{KNS} can be written as a sum of three contributions: $g^{th}_{KNS} + g^v_{KNS} + g^{duct}_{KNS}$, arising from thermal and viscous boundary layers, and the presence of a hole in the resonator wall, respectively. In a similar way, the resonance frequency shift can be written as a sum of contributions as $\Delta f_{KNS} = \Delta f^{th}_{KNS} + \Delta f^v_{KNS} + \Delta f^{duct}_{KNS}$.

Relaxation of internal vibrational degrees of freedom of a molecule can contribute to an additional half-width g_{int}, if the relaxation time is comparable to the period of the acoustic oscillation. Although the effect of internal relaxation on the half-widths can sometimes be appreciable, the resonance frequencies (and, therefore, the deduced speed of sound) are not affected and are not considered further here.

Measurements of the speed of sound in argon are used to calibrate the dimensions of the resonator and to detect energy loss mechanisms not accounted for in the present model. After subtracting the known contributions to the half-widths from the measured half-widths, the residual $\Delta g/f$ was always less than 1×10^{-4} at low pressures and increased to an average of 1.5×10^{-4} at 1000 kPa.

2.5. Perturbations: Viscothermal Boundary Layer and Duct

The effects of viscous drag and thermal conduction contribute to energy loss near the walls for all acoustic modes of a cylindrical cavity. (This is in contrast to a spherical cavity, where the purely radial modes are free from viscous boundary losses.) Viscous boundary loss occurs when the tangential component of the gas velocity is not zero near the wall of the cavity. For a radial mode in a cylindrical cavity, the velocity has a tangential component near the two ends, for a longitudinal mode the velocity has an axial component along the side, and for azimuthal modes the velocity has tangential components near the wall. For our resonator the ends made up less than 20% of the total surface area.

Mehl and Moldover [3] used first-order perturbation theory [21] to determine the effect of the thermal boundary on the radial modes in a spherical cavity. Applying this approach to a cylindrical cavity, we find that the increases in the resonance half-width due to thermal and viscous losses within the boundary layer are given by

$$g_{KNS}^{\text{th}} = \frac{f\delta_t(\gamma - 1)}{2a\Lambda(N, S)}\left[1 + \frac{a}{l}(2 - \delta(K, 0))\,\Lambda(N, S)\right] \tag{7a}$$

and

$$g_{KNS}^{\nu} = \frac{f\delta_\nu}{2a\Lambda(N, S)}\left[1 - \frac{z(N, S)^2\,\Lambda(N, S)[1 - (a/l)(2 - \delta(K, 0))]}{a^2[(K\pi/l)^2 + (z(N, S)/a)^2]}\right] \tag{7b}$$

where

$$\Lambda(N, S) = [1 - (N/z(N, S))^2][1 - \delta(N, 0)\,\delta(S, 0)] + \delta(N, 0)\,\delta(S, 0) \tag{7c}$$

The viscous and thermal penetration depths are $\delta_v = (\eta/\rho\pi f)^{1/2}$ and $\delta_t = (\kappa/\rho C_p \pi f)^{1/2}$, respectively, and we have defined the function $\delta(K, 0) = 1$ when $K = 0$ and 0 otherwise. As before, the frequency f in Eq. (7) may be taken as the resonance frequency f_{KNS} without introducing errors larger than second order in g/f. The expressions in Eq. (7) agree with an independent derivation given in Ref. 11. The shift in the resonance frequency from these perturbations is found from perturbation theory together with the kinetic theory of gases to be

$$\Delta f^{\text{th}}_{KNS} = -g^{\text{th}}_{KNS}(1 - 2l_t/\delta_t) \tag{8a}$$

and

$$\Delta f^{\text{v}}_{KNS} = -g^{\text{v}}_{KNS}(1 - 2l_v/\delta_v) \tag{8b}$$

where l_t and l_v are called the thermal and viscous accommodation lengths given by

$$l_t = (\kappa/p)(\pi MT/2R)^{1/2}\,[(2 - h_t)/h_t]/[C_v/R + 1/2] \tag{8c}$$

$$l_v = (\eta/p)(\pi RT/2M)^{1/2}\,[(2 - h_v)/h_v] \tag{8d}$$

Here, C_v is the isochoric specific heat. The accommodation coefficients h_t and h_v are empirical quantities which are dependent on the composition and condition of the wall. Experiments in spherical, stainless-steel resonators have been found to be consistent with $h_t = 1$. For the work presented here, both h_t and h_v were assumed to be 1.

The empirical method of Reichenberg, as described by Reid et al. [22], was used to estimate the viscosities η of E134 and E245. With this method η is assumed to have the form

$$\eta = \frac{a^* T_r}{[1 + 0.36 T_r (T_r - 1)]^{1/6}} \tag{9a}$$

with η in Pa · s. Here, a^* is dependent on the compound and $T_r = T/T_c$, where T_c is the critical temperature. For E134 $a^* = 17.08 \times 10^{-6}$ and $T_c = 420.25$ K [17]; for E245 $a^* = 16.24 \times 10^{-6}$ and $T_c = 444.03$ K [23]. The thermal conductivity was estimated with the modified Eücken correlation [22],

$$\kappa = \frac{\eta R}{M}\,[1.32(C^0_p/R - 1) + 1.77] \tag{9b}$$

where κ is in $W \cdot m^{-1} \cdot K^{-1}$ and M is the molar mass in $kg \cdot mol^{-1}$. These estimates for the transport properties may be in error by as much as 15%,

with corresponding errors up to 60 ppm in the speed of sound and 0.2% in the ideal-gas heat capacity.

A stainless-steel tube, 0.29 cm in inside diameter and 60 cm long (not shown in Fig. 1), was used to admit the sample gas into the resonator. The tube was coiled through the bath to provide good thermal contact. It led from a stainless-steel valve at ambient temperature to the resonator. The dimensions of the tube were a compromise between competing requirements. A narrow tube reduces the acoustic energy loss and undesirable perturbations to the resonator's modes, but it results in a low pumping speed for evacuation of the resonator. The opening into the cavity was a duct located on the same end as the transducers, a distance $b = 1.65$ cm from the cylinder axis and equally distant from the two transducers. The duct had a radius $c = 0.046$ cm and a length $l_{\text{duct}} = 2.243$ cm. From the Kirchhoff–Helmholtz (KH) theory [21], we estimated that the fractional perturbations to the resonance frequencies in our resonator were less than $\pm 15 \times 10^{-6}$ for the modes studied. These estimates were confirmed by measurement. The time constant for evacuating the resonator was about 15 minutes.

Our calculations show that the frequency shift $\Delta f_{KNS}^{\text{duct}}$ and half-width g_{KNS}^{duct} due to a hole in one end of the resonator wall located a distance b from the axis is given by

$$\Delta f_{KNS}^{\text{duct}} + i g_{KNS}^{\text{duct}} = \frac{u}{2\pi l}\left(\frac{c}{a}\right)^2 (iy_{\text{duct}})\, I(N, S) \tag{10a}$$

where

$$I(N, S) = \begin{cases} \dfrac{2}{(1+\delta(N,0))(1+\delta(K,0))\, A(N,S)} \left[\dfrac{J_N\left(z(N,S)\dfrac{b}{a}\right)}{J_N(z(N,S))}\right]^2, & \text{if } z(N,S) \neq 0 \\ 1, \quad \text{if } z(N,S) = 0 \end{cases} \tag{10b}$$

The specific acoustic admittance y_{duct} is given by

$$iy_{\text{duct}} = \frac{(\zeta^2 - 1)\tan(k_{KH} l_{\text{duct}}) + i\zeta[1 - \tan^2(k_{KH} l_{\text{duct}})]}{1 + \zeta^2 \tan^2(k_{KH} l_{\text{duct}})} \tag{10c}$$

where $\zeta = (c_t/c)^2$ and c_t is the radius of the fill tube. The wavenumber k_{KH} in a duct with surface losses is complex and is given by

$$k_{KH} = (2\pi f/u)\{1 + (1-i)[\delta_v + \delta_t(\gamma - 1)]/2c\} \tag{10d}$$

2.6. Pressure and Temperature Measurements

The resonator was placed in a temperature-controlled stirred-fluid bath which provided rapid thermal equilibration and a stability of 1 mK. A glass-encapsulated, 25-Ω standard platinum resistance thermometer (SPRT) manufactured by Leeds and Northrop (LN 1818362) was enclosed in an aluminum block attached to the outside of the resonator. The sample's temperature was inferred from the SPRT's calibration on IPTS-68 and then converted to ITS-90. Four-wire resistance measurements were performed with an ac resistance bridge for the E134 sample and with a Hewlett-Packard 3458A high-precision (8.5-digit) dc multimeter for the E245 sample.

Pressure measurements were made using a Ruska Instrument Corporation Model 6000 DPG (SN 40162) which is a differential-type quartz-bourdon-tube pressure gauge. The reference pressure was kept below 2 Pa with a rotary pump. The manufacturer's calibration stated that the gauge had an inaccuracy of less than 10 Pa over the range of the instrument (0.01 to 1000 kPa). A calibration of the pressure gauge here at NIST on Oct. 14, 1992 (3 years after purchase) using a piston gauge showed that the gauge's calibration was in error by $\Delta p/p = 1 \times 10^{-4}$. This error had a negligible effect on the results presented here. The gauge's zero indication was periodically checked by connecting the test and reference ports together while evacuated, and it was observed to drift by as much as 50 Pa during a 2-week period.

The sample gas was never admitted into the bourdon gauge. Instead, we used a diaphragm-type differential pressure transducer to separate the sample from the buffer gas. The differential pressure transducer (MKS Instruments Model 315BD-00100) was made entirely of stainless steel and was bakeable to 200 °C. The pressure transducer and the gas handling system were kept at room temperature during the acoustic measurements.

2.7. Sample Purity

The E134 sample, designated WRC-2, had a mass of 2.3 g. It was a highly purified sample loaned to us by Dr. Stephen G. Harsy of W. R. Grace & Co. Dr. Harsy used preparative gas chromatography (GC) to isolate this sample from lot 9269 manufactured by PCR, Inc., in Gainesville, Florida. Harsy provided an analysis of the sample purity in terms of gas-chromatographic area ratios. The sample was found to be 99.51 % E134 with six impurities that made up the balance of the material. The only identified impurity was R143 at a level of 0.02 %, and the largest single impurity was only 0.13 % of the sample. Assuming that γ_0 for R143

and E134 are the same, we estimated that the R143 impurity would increase the speed of sound of pure E134 by 40 ppm and decrease the ideal-gas heat capacity of pure E134 by less then 0.1%. We could not determine the influence of the other, unidentified impurities.

The composition of the E245 sample was determined using simultaneous gas chromatography and mass spectrometry. After injection of the sample into a Poraplot Q column, supplied by Chrompak Corp., the effluence was analyzed for 20 min. The impurity analysis was determined in terms of area ratios A_N/A_{E245}, where A_{E245} is the area under the peak assigned to E245. The sample was found to contain air with a GC peak area of $0.012A_{E245}$. The remaining impurities had GC peak areas of less than $0.0002A_{E245}$. Since none of these remaining impurities had been identified, we could not estimate their influence on the acoustic measurements.

Both the E134 and the E245 samples were degassed to remove air and other volatile impurities before we began the acoustic measurements. The sample was degassed by the following procedure: the sample was frozen at 77 K and its vapor pressure measured; any volatile vapor over the solid was then pumped out; the sample was then allowed to warm slightly while being cryopumped into a second vessel at 77 K; when the transfer was complete, the vapor pressure over the solid was measured again. This cycle was repeated until no appreciable change in the vapor pressure was obtained.

2.8. Measurement Procedure

Measurements of the sound speed were made at several pressures along each isotherm. When the fluid bath temperature had stabilized, the resonator was charged with the sample to the highest pressure. When the measurements at one pressure were complete, a portion of the sample was removed to reach the next desired pressure. After each change in pressure, we waited long enough (approximately 5 min) for the temperature of the sample to return to the bath's temperature before beginning the measurements. The sample's temperature and pressure were measured both before and after the acoustic measurements. This precaution provided a means of evaluating the reliability of the acoustic data.

At each state point, the speed of sound in the gas was deduced from measurements of the resonance frequencies f_{KNS} and half-widths g_{KNS} for several acoustic modes of the resonator. For each chosen mode, the signal from the detector was measured at 11 drive frequencies spanning the width of the resonance from $f_{KNS}-g_{KNS}$ to $f_{KNS}+g_{KNS}$ and then from $f_{KNS}+g_{KNS}$ to $f_{KNS}-g_{KNS}$. Performing the frequency sweep in both directions reduces the effects of small temperature or pressure drifts on the

resonance frequency. The drive voltage was generated by a frequency synthesizer and amplified with an audio amplifier. The detector signal was measured with a two-phase lock-in amplifier (Ithaco Model 393) synchronized to the drive frequency. The signal as a function of frequency for each mode (K, N, S) was fit with the theoretically expected six- or eight-parameter function to determine both f_{KNS} and g_{KNS}. The eight-parameter fit, which includes a complex linear background, was selected only when it was significant at the 95% confidence level.

2.9. Calibration

We determined the dimensions of the resonator $l(T)$ and $a(T)$ from measurements of the resonance frequencies when the cavity was filled with argon. Argon is an excellent choice because it is chemically inert and because its speed of sound and transport properties are known very well over a wide range of temperature and pressure. (The viscosity and thermal conductivity are required to calculate the corrections due to the presence of the boundary layer.) The length $l(T)$ was determined from pure longitudinal modes, and the radius $a(T)$ was determined from pure radial and/or pure azimuthal modes.

A mode-by-mode calibration with argon was performed for the E134 measurements as a means of removing small systematic inconsistencies among the modes. The calibration extended from 255 to 380 K in temperature and from 10 to 200 kPa in pressure. The calibration obtained was

$$\begin{gathered} l_{K00}(T) = A_{K00}(1 + \alpha(T - 297.206)) \\ a_{0NS}(T) = A_{0NS}(1 + \alpha(T - 297.206)) \\ \alpha = 16.077 \times 10^{-6}, \qquad A_{200} = 0.1408485, \qquad A_{300} = 0.1408372 \\ A_{400} = 0.1408436, \qquad A_{010} = 0.0327758, \qquad A_{001} = 0.0327778 \end{gathered} \tag{11a}$$

where $l_{K00}(T)$, $a_{0NS}(T)$, and A_{KNS} are in meters, α is in K^{-1}, and T is in K. For the E245 measurements, we used another resonator similar to the one used for the E134 measurements. (The first resonator filled with silicone oil when a leak developed at a compression fitting.) This second resonator had a higher-quality surface finish and tighter-fitting ends than the first resonator. A satisfactory calibration of this resonator was obtained by averaging over several modes rather than mode by mode as before. The result of the calibration used for the E245 measurements was

$$\begin{aligned} l(T) &= l_0[1 + \alpha(T - 273.15)] \\ a(T) &= a_0[1 + \alpha(T - 273.15)] \end{aligned} \tag{11b}$$

with $\alpha = 18.127 \times 10^{-6}\ \mathrm{K}^{-1}$, $a_0 = 0.0328811$ m, $l_0 = 0.1404509$ m, and T in K. This calibration covers the range from 255 to 400 K and from 10 to 1000 kPa.

3. RESULTS

3.1. Results for E134

The speed of sound was measured along each of seven isotherms at seven or eight pressures. The results are tabulated in Table I in the same order that the measurements were performed. The speed of sound quoted at each state point is the weighted average over five resonator modes. Among the modes studied, the fractional deviation of the sound speed from the average was less than 50×10^{-6}. Calibration of the resonator with argon was performed at the lower temperatures after the isotherm at 283 K. A measurement at 255 K was then repeated to test the reproducibility of the measurement and to ensure that all the argon had been removed. Calibration at the higher temperatures was performed after the isotherm at 373 K.

For each isotherm, Eq. (1) was fit to the sound-speed data by treating γ_0, β_a, and γ_a as adjustable parameters. The molar mass of E134 is $0.118031\ \mathrm{kg \cdot mol^{-1}}$. Equation (2) was then used to determine C_p^0. The results of these fits are shown in Table II. The range of pressures encompassed by the data below 300 K are a significant fraction of the saturation pressure, and for these isotherms we could obtain values for both the second and third acoustic virial coefficients. Above 300 K the pressure range was too small to justify more than a linear fit in p, hence the entries for γ_a are omitted in Table II for these temperatures. The lower portion of Fig. 3 shows a plot of the sound speed as a function of pressure for the data in Table I. The upper portion of Fig. 3 shows the deviations of the sound speed from a surface described below.

The heat capacities in Table II were fit with a polynomial expression in the temperature T. Inclusion of a cubic temperature dependence in the fit to $C_p^0(T)$ was justified by an F test at the 93% confidence level with the result

$$C_p^0/R = c_0 + c_1 t + c_2 t^2 + c_3 t^3 \tag{12}$$

where

$$c_0 = 11.1251$$

$$c_1 = 0.032143\ \mathrm{C}^{-1}$$

$$c_2 = -1.6095 \times 10^{-4}\ \mathrm{C}^{-2}$$

$$c_3 = 6.660 \times 10^{-7}\ \mathrm{C}^{-3}$$

Table I. Measured Speed of Sound in E134

T (K)	p (kPa)	u ($m \cdot s^{-1}$)	$10^6 (\Delta u/u)^a$
255.06	26.08	139.326	91.7
	19.35	139.747	79.4
	15.93	139.959	71.5
	13.20	140.127	62.3
	10.20	140.311	53.8
	7.27	140.490	46.5
268.04	49.86	141.487	−97.9
	39.87	142.028	−105.0
	28.87	142.616	−117.0
	20.49	143.057	−139.0
	13.86	143.403	−156.0
	8.39	143.687	−166.0
283.90	71.12	144.907	132.0
	59.00	145.453	117.0
	49.96	145.858	115.0
	39.74	146.309	90.9
	29.90	146.740	70.5
	19.88	147.176	54.8
	14.95	147.390	52.6
	10.44	147.587	64.1
255.07	26.17	139.307	−42.8
313.77	76.71	152.727	−82.7
	49.76	153.590	−33.2
	30.60	154.195	−35.0
	24.87	154.376	−32.1
	15.04	154.686	−27.3
	9.22	154.872	−6.7
335.66	80.70	158.149	−36.5
	60.28	158.679	−17.2
	40.55	159.183	−39.0
	29.77	159.460	−36.4
	23.96	159.611	−23.1
	16.03	159.818	2.1
	9.39	159.991	22.4
357.13	84.36	163.253	25.9
	60.62	163.756	−5.5
	40.01	164.197	1.5
	29.88	164.407	−33.5
	23.72	164.537	−40.0
	16.26	164.698	−25.3
	9.27	164.851	2.3
373.83	87.24	167.075	33.1
	60.49	167.572	15.1
	40.18	167.943	−30.4
	29.65	168.138	−36.2
	22.15	168.277	−38.8
	14.59	168.428	23.9
	8.23	168.553	65.1

[a] The fractional deviation of u from the surface fit shown in Fig. 3.

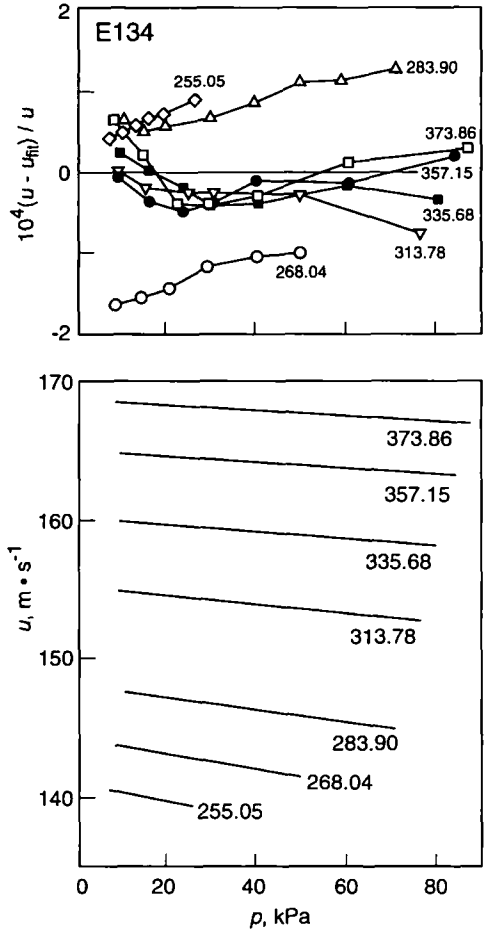

Fig. 3. Below: Speed of sound $u(T, p)$ in E134 as a function of pressure from Table I. Above: Deviations of $u(T, p)$ in E134 from the surface defined in the text. Temperatures are in K.

and where t is in °C. The deviations of C_p^0 from Eq. (12) are listed in Table II. The standard deviation is $0.002R$, giving a fractional deviation of 0.13%. The ideal-gas heat capacity C_p^0 and the fractional deviations of C_p^0 from Eq. (12) are shown in Fig. 4.

The acoustic virial coefficients obtained from the isotherm fits to the speed of sound are listed in Table II. Figure 5 shows the second acoustic virial coefficient β_a as a function of T. The third acoustic virial coefficients

Table II. Ideal-Gas Heat Capacities C_p^0, Second Virial Coefficients β_a, and Third Virial Coefficients γ_a for E134 from Isotherm Fits[a]

T (K)	C_p^0/R	$\Delta C_p^0/R$	$\delta C_p^0/R$	β_a	$\Delta\beta_a$ ($cm^3 \cdot mol^{-1}$)	$\delta\beta_a$	γ_a ($cm^3 \cdot mol^{-1} \cdot kPa^{-1}$)
255.06	10.484	−0.004	0.003	−1811.0	12.0	7.0	−1.05
268.04	10.997	0.040	0.009	−1579.0	14.0	15.0	−0.64
283.90	11.441	−0.010	0.008	−1362.0	4.0	9.0	−0.37
313.77	12.205	0.000	0.008	−1059.0	−5.0	9.0	—
335.66	12.661	0.000	0.004	−891.9	−3.0	2.0	—
357.13	13.087	0.013	0.009	−759.7	3.0	4.0	—
373.83	13.397	−0.002	0.010	−683.0	0.0	4.0	—

[a] ΔC_p^0 is the deviation from Eq. (12) and $\Delta\beta_a$ is the deviation from the surface defined in the text. δC_p^0 and $\delta\beta_a$ are standard deviations from the isotherm fits.

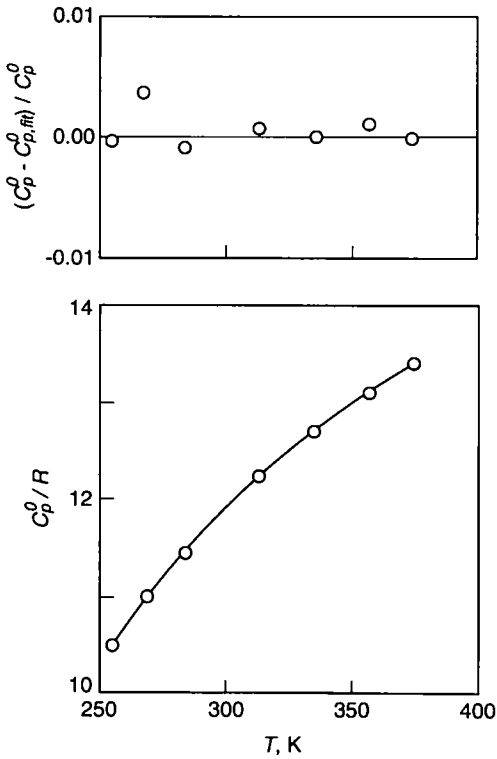

Fig. 4. Below: Ideal-gas heat capacities $C_p^0(T)$ for E134 from fits of Eq. (1) to speed-of-sound data. Above: Deviations of $C_p^0(T)$ from Eq. (12).

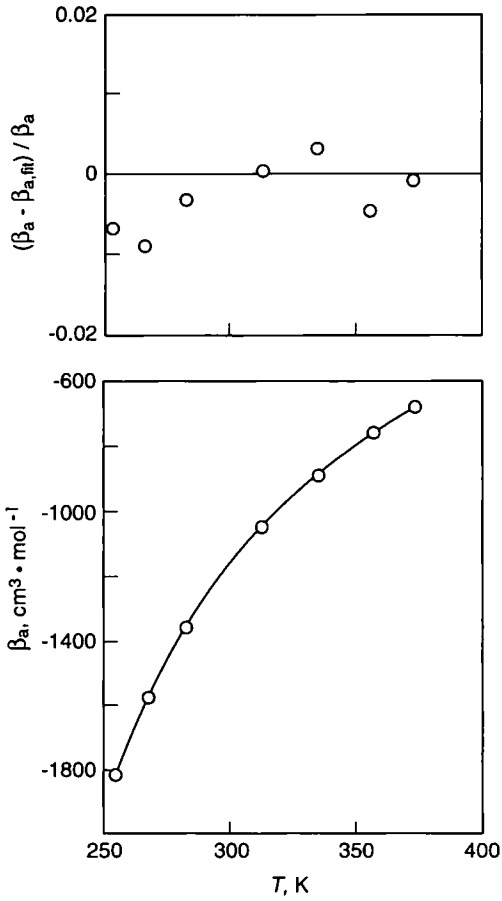

Fig. 5. Below: Second acoustic virial coefficients $\beta_a(T)$ for E134 obtained from isotherm fits of Eq. (1) to speed-of-sound data. Above: Deviations of $\beta_a(T)$ from Eq. (4) with $B(T)$ given by Eqs. (14) and (16).

obtained for the lowest three isotherms are also given in Table II. The connection between β_a and the second virial coefficient B was made using Eq. (4), assuming a square-well intermolecular potential [24]:

$$U(r) = \begin{cases} \infty, & r < \sigma \\ -\varepsilon, & \sigma < r < \lambda\sigma \\ 0, & r > \lambda\sigma \end{cases} \tag{13}$$

where r is the distance between molecular centers, ε is the well depth, σ is the hard-core radius, and λ is the ratio of the width of the well to the width of the hard core. The relationship between the square-well parameters and the second virial coefficient B from the equation of state is

$$B(T) = b_0[1 - (\lambda^3 - 1)\,\Delta] \tag{14}$$

where

$$\Delta = e^{\varepsilon/kT} - 1$$

$b_0 = 2\pi N_a \sigma^3$ is the hard-core molar volume, and N_a is Avogadro's number. Equations (4), (12, and (14) define a surface which was fit to all of the speed-of-sound data simultaneously. For this fit the third acoustic virial was represented by the function

$$\begin{aligned} \gamma_a(T) &= -3.4 \times 10^{14} \exp(2635/T) \qquad \text{for} \quad T < 290\ \text{K} \\ &= 0 \qquad\qquad\qquad\qquad\quad \text{for} \quad T > 290\ \text{K} \end{aligned} \tag{15}$$

where $\gamma_a(T)$ is in $m^3 \cdot mol^{-1} \cdot Pa^{-1}$ and T is in K. The third acoustic virial was set to zero for $T > 290$ K because the exponential function, extrapolated beyond the fitting region, predicts values of $|\gamma_a|$ that are too large. The square-well parameters obtained from the surface fit were

$$\begin{aligned} b_0 &= 50.74\ \text{cm}^3 \cdot \text{mol}^{-1} \\ \lambda &= 1.355 \\ \varepsilon &= 736.4\ \text{K} \end{aligned} \tag{16}$$

The deviations of β_a from the best-fit square-well model are given in Table II, and the fractional deviations are shown in Fig. 5. No independent measurements of β_a or B exist that could be compared to the results given here. Fractional deviations of $u(T, p)$ from the surface are all less than 2×10^{-4}, as shown in the upper portion of Fig. 3.

Alternatively, the square-well parameters could be determined from a direct fit to the second acoustic virial coefficients (obtained from the isotherm fits) rather than a surface fit to all the data. Due to the fewer number of degrees of freedom present with this type of fit, the surface fit was chosen as the preferred method.

3.2. Results for E245

The speed of sound in E245 was measured at several pressures on five isotherms. To avoid precondensation effects at the lowest temperature, the

Table III. Measured Speed of Sound in E245

T (K)	p (kPa)	u ($m \cdot s^{-1}$)	$10^6 (\Delta u/u)^a$
277.61	20.29	126.886	29.8
	18.06	127.041	46.8
	16.09	127.170	−8.1
	14.32	127.293	13.8
	11.93	127.456	2.0
297.70	49.46	129.928	−60.4
	43.41	130.260	−46.0
	36.27	130.652	−15.6
	28.21	131.090	−6.9
	21.90	131.435	24.4
321.31	49.84	135.453	51.6
	34.72	136.091	48.6
	20.13	136.698	5.6
339.55	49.72	139.486	16.6
	34.64	140.017	−3.9
	24.28	140.383	−3.5
384.40	50.32	148.731	−14.9
	43.07	148.910	1.0
	35.13	149.099	−22.1
	28.56	149.261	−2.0
	22.64	149.405	5.0
	14.63	149.598	1.1

[a] The fractional deviation of u from the surface shown in Fig. 6.

maximum pressure was limited to 60% of the vapor pressure. For the other isotherms, the maximum pressure was limited by the vapor pressure at room temperature. At 400 K the E245 reacted within our apparatus. The gas pressure within the resonator was observed to rise by several percent over 8 h. The acoustic data obtained at this temperature were discarded as unreliable. No reaction was observed at lower temperatures. The measured sound speeds, representing an average over two modes, are given in Table III. The fractional uncertainty in the speed-of-sound measurement was ± 0.00015. The fractional deviation from a surface fit, to be discussed below, is also given in Table III. A plot of the sound speed as a function of pressure is shown in the bottom graph in Fig. 6.

Because of the limited pressure range, we found that the third acoustic virial coefficient in Eq. (1) was not needed to fit the data in Table III. The ideal-gas heat capacity and the second acoustic virial coefficient obtained from a fit to each isotherm are given in Table IV. (The molar mass of E245 is $0.150048\ kg \cdot mol^{-1}$). The uncertainty in the determination of the heat

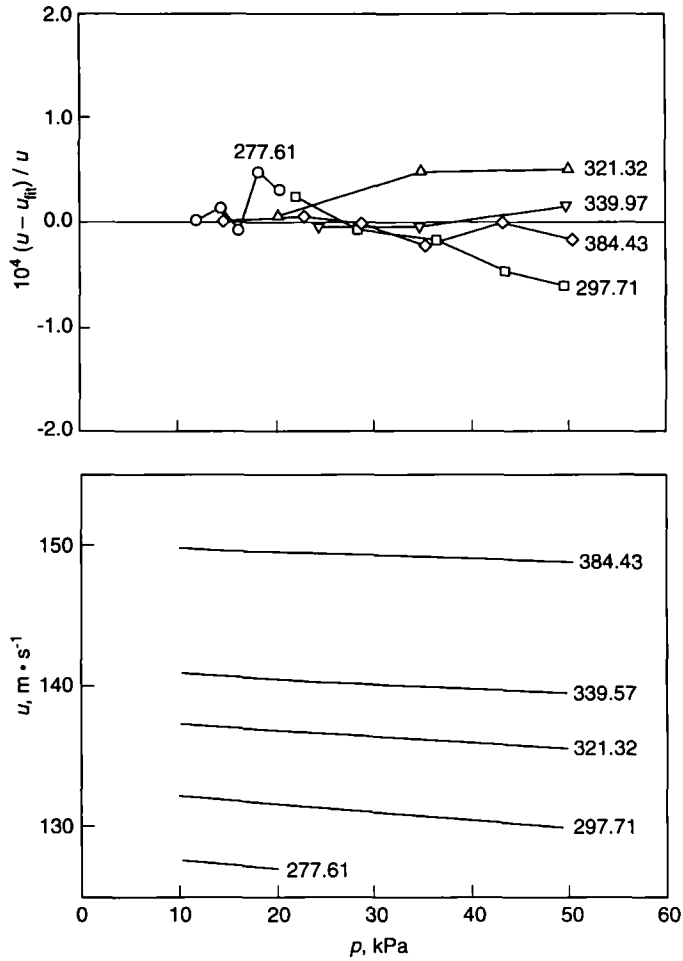

Fig. 6. Below: Speed of sound $u(T, p)$ in E245 as a function of pressure from Table III. Above: Deviations of $u(T, p)$ in E245 from the surface defined in the text. Temperatures are in K.

capacity was estimated to be $\pm 0.003 C_p^0$. The heat capacities in Table IV were fit by Eq. (12) to represent the temperature dependence. The results of a two-term fit are

$$c_0 = 15.312$$
$$c_1 = 0.03383 °C^{-1} \tag{17a}$$

Table IV. Ideal-Gas Heat Capacities C_p^0 and Second Virial Coefficients β_a for E245 from Isotherm Fits[a]

T (K)	C_p^0/R	$\Delta C_p^0/R$	$\delta C_p^0/R$	β_a	$\Delta\beta_a$ (cm^3·mol^{-1})	$\delta\beta_a$
277.61	15.40	0.019	0.04	−2426.0	3.1	11.0
297.70	16.11	−0.039	0.02	−2011.0	−13.6	3.0
321.31	17.01	0.009	0.05	−1611.0	12.2	9.0
339.55	17.63	0.015	0.05	−1395.0	7.4	9.0
384.40	18.97	−0.005	0.04	−1030.0	−10.8	8.0

[a] ΔC_p^0 is the deviation from Eqs. (12) and (17b) and $\Delta\beta_a$ is the deviation from the surface defined in the text. δC_p^0 and $\delta\beta_a$ are standard deviations from the isotherm fits.

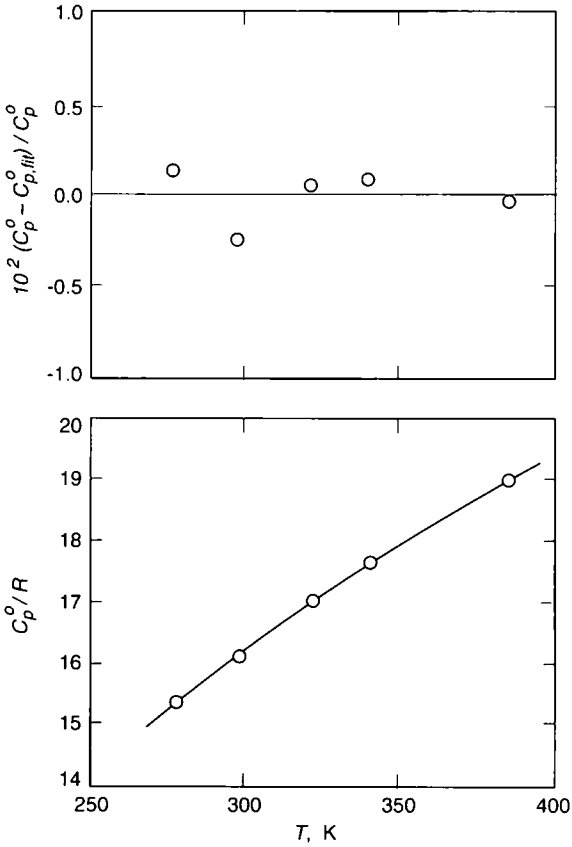

Fig. 7. Below: Ideal-gas heat capacities $C_p^0(T)$ for E245 from fits of Eq. (1) to speed-of-sound data. Above: Deviations of $C_p^0(T)$ from Eqs. (12) and (17b).

with a standard deviation of $0.091R$. A three-term fit resulted in a three-fold reduction in the standard deviation

$$c_0 = 15.201$$
$$c_1 = 0.04024\ \mathrm{C}^{-1} \tag{17b}$$
$$c_2 = -5.46 \times 10^{-5}\ \mathrm{C}^{-2}$$

with a standard deviation of $0.033R$. Plots of the heat capacity and the deviation from the three-term fit are shown in Fig. 7.

The second acoustic virial coefficients β_a obtained from the isotherm fits were correlated with a hard-core square-well model, Eqs. (13) and (14). When all three parameters of the square-well potential were fit to the data, unphysical values for the width parameter λ resulted. Therefore, we chose to fix λ and adjust b_0 and ε for the best fit. When λ was fixed at the value obtained for 1,1,1,2-tetrafluoroethane (R134a) [12], the results were

$$b_0 = 85.82\ \mathrm{cm}^3 \cdot \mathrm{mol}^{-1}$$
$$\lambda = 1.296 \tag{18}$$
$$\varepsilon = 782.0\ \mathrm{K}$$

with a standard deviation of $17\ \mathrm{cm}^3 \cdot \mathrm{mol}^{-1}$. Fixing λ at the value obtained for E134 gave a slightly better but not statistically significant fit.

A surface fit using all of the speed-of-sound data from E245 was performed to determine the interaction parameters for the square-well potential. For this surface the ideal-gas heat capacity was represented by the three-term fit given above. The results of this surface fit were

$$b_0 = 16.18\ \mathrm{cm}^3 \cdot \mathrm{mol}^{-1}$$
$$\lambda = 1.765 \tag{18b}$$
$$\varepsilon = 857.0\ \mathrm{K}$$

with a standard deviation in β_a of $11\ \mathrm{cm}^3 \cdot \mathrm{mol}^{-1}$ and a standard deviation in the sound speed from the surface of $0.003\ \mathrm{m} \cdot \mathrm{s}^{-1}$. Fractional deviations of the speed of sound in E245 from the surface are shown in Fig. 6.

4. DISCUSSION AND CONCLUSIONS

Although the square-well potential represented by Eq. (13) is simple in form, it has features that are characteristic of small, nearly spherical molecules. Indeed, the square-well potential has been used to correlate

second acoustic virial coefficients with high precision for several spherical and slightly nonspherical molecules such as argon, methane, R134a, and others. In addition, estimates of second density virial coefficients were obtained for these compounds that compare exceptionally well with those obtained from PVT measurements [8–14, 25]. For extremely nonspherical molecules, especially those that have a large permanent dipole moment, we no longer expect the square-well model to be adequate for estimating B. The two compounds E134 and E245, which are the topic of this paper, may fall into this category. For this reason, we investigated an alternative means of correlating $\beta_a(T)$ using an extended corresponding-states method proposed by Pitzer and Curl [26, 27] for the reduced second density virial coefficient $p_c B/RT_c$

$$Bp_c/RT_c = A_0 - A_{-1}T_r^{-1} - A_{-2}T_r^{-2} - A_{-3}T_r^{-3} - A_{-8}T_r^{-8} \quad (19a)$$

with

$$A_0 = 0.1445 + 0.073\omega, \qquad A_{-1} = 0.330 - 0.46\omega, \qquad A_{-2} = 0.1385 + 0.50\omega$$

$$A_{-3} = 0.0121 + 0.097\omega, \qquad A_{-8} = 0.0073\omega, \qquad T_r = T/T_c$$

The acentric factor ω, which is a measure of the deviation from a spherically symmetric potential, is defined as

$$\omega = -\log(p_{0.7}/p_c) - 1.000 \quad (19b)$$

where p_c is the critical pressure and $p_{0.7}$ is the vapor pressure at $T = 0.7T_c$. Values of p_c, T_c, and ω for E134, E245, and other compounds are listed in Table V.

Table V. Properties Used in Eqs. (19) and (20) for Fig. 8[a]

Compound	T_c (K)	p_c (MPa)	ω	μ (Debye)
Argon [26]	150.80	4.87	−0.002	0.0
Ethane [25]	305.42	4.88	0.099	0.0
Propane [25]	369.82	4.250	0.153	0.0
R134a [28, 29]	374.30	4.067	0.326	2.058
E134 [17, 30]	420.25	4.228	0.367	1.739
E245 [23, 31]	444.03	3.420	0.421	0.804

[a] The dipole moment μ is included for comparison.

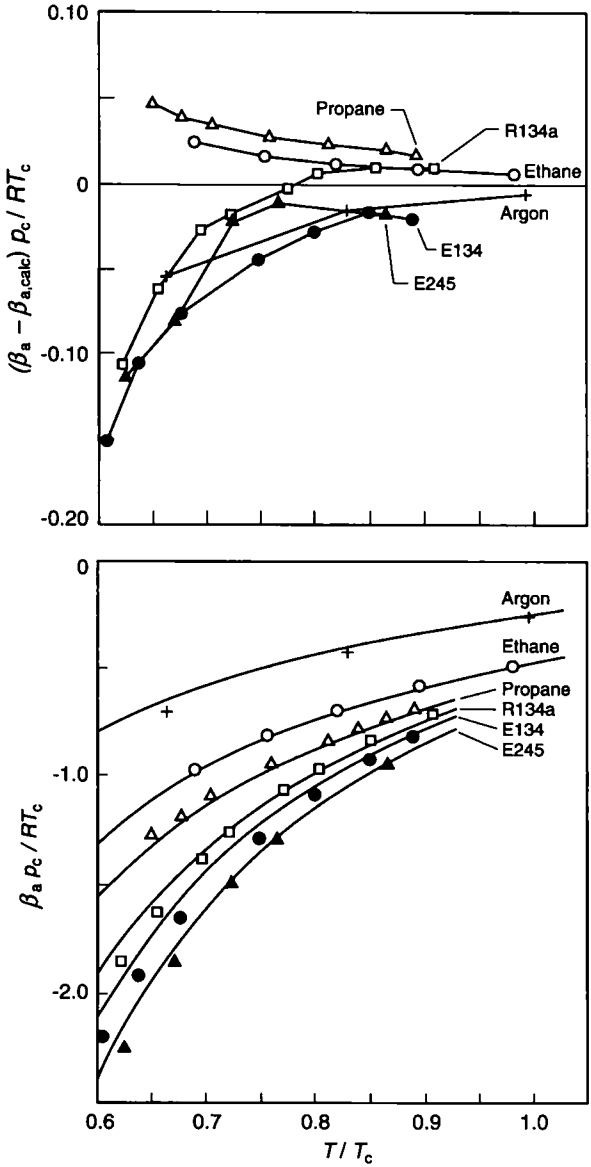

Fig. 8. Below: Reduced second acoustic virial coefficients $\beta_a p_c/RT_c$ as a function of T/T_c for argon (+) [10], ethane (○) [25], propane (△) [25], R134a (□) [12], E134 (●) (this work), and E245 (▲) (this work). The solid curves are estimates from the Pitzer and Curl correlation [Eq. (20)] using data from Table V. Above: Deviations of the measured reduced second acoustic virial coefficients $\beta_a p_c/RT_c$ from Eq. (20).

Using Eqs. (19) and (4) together with γ_0 obtained from our measurements, we obtained a means of predicting $\beta_a(T)$ from the original Pitzer and Curl correlation

$$\beta_a p_c/RT_c = \mathscr{A}_0 - \mathscr{A}_{-1} T_r^{-1} - \mathscr{A}_{-2} T_r^{-2} - \mathscr{A}_{-3} T_r^{-3} - \mathscr{A}_{-8} T_r^{-8} \quad (20)$$

$$\mathscr{A}_0 = 2A_0, \qquad \mathscr{A}_{-1} = 2A_{-1}/\gamma_0, \qquad \mathscr{A}_{-2} = -6A_{-2}(\gamma_0^2 + \gamma_0 - 1)/\gamma_0$$

$$\mathscr{A}_{-3} = 2A_{-3}(3\gamma_0^2 - 8\gamma_0 + 6)/\gamma_0, \qquad \mathscr{A}_{-8} = 2A_{-8}(28\gamma_0^2 - 63\gamma_0 + 36)/\gamma_0$$

Figure 8 shows a comparison of $\beta_a p_c/RT_c$ obtained from acoustic measurements and Eq. (20) as a function of T_r for E134, E245, and several other compounds. This plot shows that $\beta_a(T)$ for both polar and nonpolar molecules can be predicted to within a few percent knowing only ω, p_c, T_c, and $\gamma_0(T)$.

ACKNOWLEDGMENTS

We thank Dr. Stephen G. Harsy of W. R. Grace & Co. for lending us the purified E134. We also thank Steven J. Boyes for calibrating the Ruska pressure gauge. This work was sponsored, in part, by the U.S. Department of the Navy under Contract N0002490MP33493 and by the U.S. Environmental Protection Agency under Contract DW13935108-01-0.

REFERENCES

1. *Montreal Protocol on Substances that Deplete the Ozone Layer: Final Act*, United Nations Environmental Programme (UNEP), Sept. 16 (1987).
2. M. R. Moldover, M. Waxman, and M. Greenspan, *High Temp. High Press.* **11**:75 (1979).
3. J. B. Mehl and M. R. Moldover, *J. Chem. Phys.* **74**:4062 (1981).
4. J. B. Mehl and M. R. Moldover, in *Proc. Eighth Symp. Thermophys. Prop.*, J. V. Sengers, ed. (Am. Soc. Mech. Eng., New York, 1982), pp. 134–141.
5. M. R. Moldover, J. B. Mehl, and M. Greenspan, *J. Acoust. Soc. Am.* **79**:253 (1986).
6. M. R. Moldover, J. P. M. Trusler, T. J. Edwards, J. B. Mehl, and R. S. Davis, *J. Res. Natl. Bur. Std.* **93**:85 (1988).
7. A. R. H. Goodwin, Ph.D. thesis (Chemistry Department, University of London, London, 1988) (unpublished).
8. S. J. Boyes, M. B. Ewing, and A. R. H. Goodwin, *J. Chem. Thermodynam.* **24**:1151 (1992), and references cited therein.
9. M. B. Ewing and J. P. M. Trusler, *J. Chem. Phys.* **90**:1106 (1989).
10. M. B. Ewing, A. A. Owusu, and J. P. M. Trusler, *Physica A* **156**:899 (1989).
11. J. P. M. Trusler, *Physical Acoustics and Metrology of Fluids* (Adam Hilger, Bristol, 1991).
12. A. R. H. Goodwin and M. R. Moldover, *J. Chem. Phys.* **93**:2741 (1990).
13. A. R. H. Goodwin and M. R. Moldover, *J. Chem. Phys.* **95**:5230 (1991).
14. A. R. H. Goodwin and M. R. Moldover, *J. Chem. Phys.* **95**:5236 (1991).
15. M. B. Ewing and A. R. H. Goodwin, *J. Chem. Thermodyn.* **23**:1107 (1991).

16. M. B. Ewing and A. R. H. Goodwin, *J. Chem. Thermodyn.* **24**:301 (1992).
17. D. Defibaugh, K. A. Gillis, M. R. Moldover, G. Morrison, and J. W. Schmidt, *Fluid Phase Equil.* **81**:285 (1992).
18. K. A. Gillis, A. R. H. Goodwin, and M. R. Moldover, *Rev. Sci. Instrum.* **62**:2213 (1991).
19. W. L. Kopko, in *Proceedings of ASHRAE's 1989 CFC Technology Conference*, Gaithersburg, MD, Sept. 27–28 (ASHRAE, Atlanta, 1989, GA), pp. 39–46.
20. J. W. S. Rayleigh, *Theory of Sound* (Dover, New York, 1945).
21. P. M. Morse and K. U. Ingard, *Theoretical Acoustics* (McGraw-Hill, New York, 1968), see Sect. 6.4, 9.1.
22. R. C. Reid, J. M. Prausnitz, and T. K. Sherwood, *The Properties of Gases and Liquids*, 3rd ed. (McGraw-Hill, New York, 1977), pp. 404, 474; *ibid.*, 4th ed., Section 10-9.
23. J. W. Schmidt, personal communication.
24. G. C. Maitland, M. Rigby, E. B. Smith, and W. A. Wakeham, *Intermolecular Forces* (Clarendon Press, Oxford, 1981), p. 122.
25. S. J. Boyes, M. B. Ewing, and A. R. H. Goodwin, Virial Coefficients for C_1-C_5 alkanes from Speed of Sound Measurements, Joint Meeting of the 12th IUPAC Conference on Chemical Thermodynamics and the 47th Calorimetry Conference, Snowbird, UT, Aug. (1992), and private communication.
26. See Ref. 24, p. 152 and Appendices 5 and 6.
27. K. S. Pitzer and R. F. Curl, Jr., *J. Am. Chem. Soc.* **79**:2369 (1957).
28. A. R. H. Goodwin, D. R. Defibaugh, and L. A. Weber, *Int. J. Thermophys.* **13**:837 (1992).
29. C. W. Meyer and G. Morrison, *J. Phys. Chem.* **95**:3860 (1991).
30. C. W. Meyer and G. Morrison, *J. Chem. Eng. Data* **36**:409 (1991).
31. A. R. H. Goodwin and G. Morrison, *J. Phys. Chem.* **96**:5521 (1992).